RSC Advances

PAPER

View Article Online
View Journal | View Issue

Cite this: *RSC Adv.*, 2022, **12**, 33737

Towards optimization of mechanical and microstructural performances of Fe-rich laterite geopolymer binders cured at room temperature by varying the activating solution

Rodrigue Cyriaque Kaze, *[ab] Juvenal Giogetti Deutou Nemaleu, [b] Elie Kamseu,*[bc] Florence Uphie Chinje,[a] Fernanda Andreola[c] and Cristina Leonelli [c]

In the present study, the performances of the end products prepared using calcined iron-rich laterite at 600 °C (LAT600) with different alkaline solution (AS) to calcined laterite (AS/LAT600) mass ratio (0.45–0.65) were investigated. The effect of AS/LAT600 mass ratio on microstructural and mechanical properties of consolidated geopolymer samples, such as compressive strength, porosity, bulk density, water absorption, mercury intrusion porosimetry (MIP) and scanning electron microscopy (SEM) analysis were determined. Geopolymer made with AS/LAT600 ratio of 0.55 yields the highest compressive strength (54 ± 0.38 MPa) and compact structure. Increasing the AS/LAT600 mass ratio (0.45–0.65) increased the setting time, flowability and decreased the SiO_2/Fe_2O_3 and Al_2O_3/Fe_2O_3 molar ratios and compressive strength leading to a weak structure. Both cumulative volume intrusion and cumulative pore area increased from 0.11 to 0.20 mL g^{-1} and 65.20 to 90.93 m^2 g^{-1}, respectively. Such enhancement is linked to changes that occur into the geopolymer network when high alkaline activator/laterite is used. Therefore, further increase of AS/LAT600 mass ratio improved the workability, delaying the polycondensation rate of dissolved calcined laterite and not positively affecting the mechanical strength development. Nevertheless, the performance of the end products could be found application in building engineering.

Received 26th August 2022
Accepted 15th November 2022

DOI: 10.1039/d2ra05365a

rsc.li/rsc-advances

1. Introduction

The research conducted on the development and production of alkali activated cementitious materials, known as alternatives to widely used ordinary Portland cement, has largely increased and gained more attraction these recent years possibly due to many advantages and interesting properties. Among these alkali activated materials, geopolymers defined by their Al_2O_3 + SiO_2 content above 80 wt%[1] appear as one of promising alternative to Portland cement. Geopolymers offer best properties in terms of low energy requirements and the low CO_2 emission,[2] the fire-resistance,[3–5] and other desired characteristics depending on the nature of solid precursor and the conditions of synthesis.[6] Last but not least, these binders exhibit good resistance in aggressive environments (*i.e.*, acidic and salty media).[7,8] Geopolymerization is a process that involves the dissolution of reactive components of the solid precursors (*e.g.*, metakaolin, slag, fly ash, volcanic ash and laterite) in an alkaline or acid media followed by polycondensation and polymerization steps towards the formation of a 3-D compact structure.[7,9–11] A possible reaction sequence is presented below:

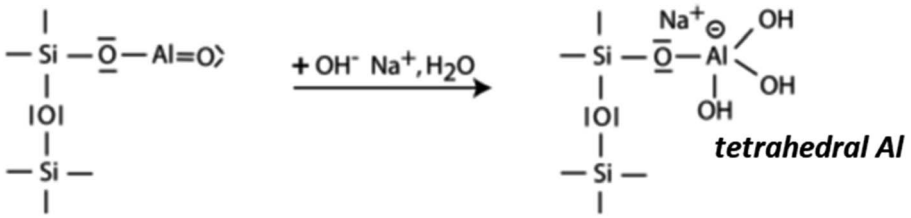

(1)

[a]*Laboratory of Applied Inorganic Chemistry, Faculty of Science, University of Yaoundé I, P.O. Box 812, Yaoundé, Cameroon. E-mail: kazerodrigue@gmail.com*

[b]*Laboratory of Materials, Local Materials Promotion Authority, MINRESI/MIPROMALO, P.O. Box 2396, Yaoundé, Cameroon. E-mail: kamseuelie2001@yahoo.fr*

[c]*Department of Engineering "Enzo Ferrari" University of Modena and Reggio Emilia, Via P. Vivarelli 10, Modena 41125, Italy*

The first step is the nucleophilic attack of OH^- on Al atom with the formation of a tetrahedral Al with a Na^+ in the role of charge balancing cation.

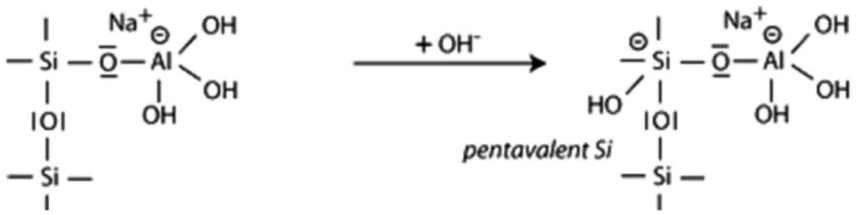

(2)

The second step is the attack of OH^- on the Si atom with the formation of a pentavalent Si which started its hydration.

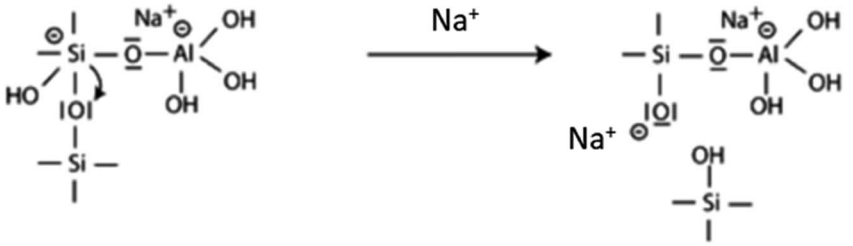

(3)

At this point the destabilization of the aluminosilicate network is at its maximum and the siloxanic bridge: Si–O–Si is broken with the formation of one silanol –Si–OH and one siloxo Si–O^- species. The disruption of the structure can continue till the formation of $Si(OH)_4$ and $Al(OH)_4$ monomers.[12]

Many factors, such as the level of dissolution and reactivity of solid precursor ratio,[13] the curing temperature and the reagent types,[10,14–16] are determinants for the entire sequence of the geopolymerization reactions and the end properties of the resulting binders. From the above-mentioned parameters affecting the characteristics of geopolymer binders, the liquid to solid ratio defining the quantity of binder formed is among the key parameters which greatly influence the resulting properties of geopolymer specimens.[12,13,17–22]

Up to date, many researches were focused on the effect of solid/liquid ratio on some fresh and hardened properties of kaolin, metakaolin, fly ashes, volcanic ash taking into account the chemistry and mineralogy. For instance, Heah *et al.*[23] produced geopolymers using kaolinite clay by varying the solid to liquid ratios. After investigations, they found that the workability decreased with the rise of solid to liquid ratio while the mechanical properties increased from 1 to 90 days. Cheng *et al.*[13] in their findings replaced metakaolin with waste catalyst up to 40 wt% and used different solid-to-liquid ratios from 0.66 to 0.81. They discovered that increasing the solid/liquid ratio reduced the porosity within the geopolymer samples resulting in an improvement of mechanical performances at early and later ages. In the same vein Liew *et al.*[21] used calcined kaolin (700 °C) and varied the solid/liquid ratios from 0.40 to 1.20 in order to find the best ratio expecting to ensure the high strength. From their study 0.8 appears as the optimum solid/liquid ratio that ensured the best mechanical performance with compact and dense structure. Recently Vogt *et al.*[17] studied the influence of solid/liquid ratio on some properties of metakaolin-fly ash blended geopolymer. They found that at higher solid/liquid ratios with high fly ash content, the total heat evolved from isothermal conductivity calorimetry (ICC) analysis decreased for the first 24 h of reaction. Taking into account the above-listed studies, it could be concluded that applying the different liquid/solid ratios for the synthesis of geopolymer remarkably affects the end properties of the resulting geopolymer products. However, it should be noted that the ratio is closely linked to the reactive fraction and the chemical composition. Thus, for a metakaolin rich in alumina, the quantity of alkaline solution consumed will be higher than for a siliceous metakaolin or fly ash.

The production of geopolymer materials from calcined or raw laterite had gained more attention, because laterite does not require high energy for thermal activation as standard kaolin.[24–26] In developing countries laterite soils are mostly used either in production of stabilized earth block made from laterite soils with conventional cement (OPC) or aggregates in Portland cement mortars and concretes.[27–30] One of advantages of using laterite as solid precursor is its availability at the surface in tropical areas.[26,31,32] Several studies were conducted on the development of geopolymer from laterites and the influences of the following parameters, silica modulus namely (SiO_2/Na_2O and H_2O/Na_2O), calcination temperature (from 25 to 1000 °C), activating solution, the pre-curing time (4–24 h), the curing temperature (25–80 °C) and the curing time (24 or 48 h) on the mechanical and microstructural properties of the geopolymers were evaluated.[10,11,14,15,33–40] For example, Kaze *et al.*[10,14,33] investigated and discussed the effect of silica modulus, curing

temperature, activator types and calcination temperature upon strength development, setting time and microstructure of geopolymer binder from calcined corroded laterite at 600 °C with solid/liquid ratio maintained at 0.6 allowing acceptable workability. Later Lemougna *et al.*[38] replaced the calcined laterite with calcite and ground granulated blast furnace slag up to 20 and 50 wt% and consolidated with alkaline activators with silica modulus ranging between 1.6 and 2.2. However, for the formulated geopolymer samples the mechanical properties increased with the reduction in silica modulus of alkaline activator, even though the solid/liquid ratio of 0.62 was used in all the formulations. Komnitsas *et al.*[39] calcined the residues of Ni-rich laterite acid leaching at 800 and 1000 °C and activated with an alkaline solution. They found that the calcination of residues at 800 and 1000 °C was not beneficial on alkali activation exhibiting low strength (1.4 MPa). However, incorporating 10 wt% of metakaolin resulted in noticeably higher compressive strength (41 MPa). The same authors[41] demonstrated that increasing the alkali activation of calcined laterite residues an Al source is required. Recently Nkawju *et al.*[42] maintained the solid/liquid ratio of 0.6 in the production of the calcined corroded laterite geopolymer containing the sugarcane fibre up to 7.5 wt%. Bewa *et al.*[43] investigated the effect of liquid to solid on fresh and hardened properties of calcined iron-rich laterite based geopolymer using phosphoric acid at different molarity. They found that varying the liquid to solid ratio positively influenced the end properties of geopolymer products mostly the mechanical and microstructural performance exhibiting a compact and dense structure.

Even though the interesting performances were obtained from the studies conducted on laterite based geopolymers, the influence of solid (aluminosilicate precursor)/liquid (alkaline solution) ratio as an important parameter of geopolymer process has been not reported yet in alkaline media. Therefore, the present work aims to evaluate the impact of solid/liquid ratio ranged between 0.45 and 0.65 on the fresh (workability, rheology and setting time) and hardened (mechanical strength, water absorption, porosity and bulk density) properties of iron-rich laterite based geopolymer. In addition, the raw materials and consolidated geopolymers with an alkaline solution were characterized using X-ray diffraction (XRD), Fourier transform infrared spectroscopy (FTIR), scanning electron microscopy (SEM) and mercury intrusion porosimetry (MIP) analyses. Finally, the obtained results were interpreted correlating the properties of fresh and hardened products.

2. Materials and methods

2.1 Materials

The laterite used as solid precursor for the binder preparation was collected in Yaoundé, Cameroon. This laterite was previously characterized by Kaze *et al.*[10] to be mainly composed of 49 Fe_2O_3, 20 SiO_2 and 17 Al_2O_3 (wt%). The collected laterite was oven dried for 48 h to eliminate moisture, afterward grinding and sieving operations resulted in a powder with a particle size of below 80 μm. Such powder was calcined at 600 °C for 4 h with 5 °C min^{-1} according to previous works.[14,15] The raw and calcined laterites were labelled LAT and LAT600, respectively.

The alkaline solution was prepared by mixing an aqueous NaOH solution (10 M from dissolution of pellets with 99% of purity) with commercial sodium silicate solution (composed of 14.37 wt% Na_2O, 29.54 wt% SiO_2 and 56.09 wt% H_2O, provided by Ingessil, Verona, Italy) in weight sodium silicate to NaOH solution ratio of 2 according to previous works.[10] The prepared alkaline solution (AS) was kept at room temperature for 24 h before being used.

2.2 Geopolymer binder's synthesis

The fresh geopolymer pastes were obtained by mixing for 5 min the calcined laterite with the alkaline solution by varying the liquid AS/solid ratio of 0.45, 0.50, 0.55, 0.60, and 0.65 (wt/wt). Afterwards the obtained pastes were poured into cylindrical silicone moulds with dimension of 60 mm (height) × 30 mm (diameter). After moulding, the specimens were sealed with a thin plastic sheet and kept at room temperature for 24 h. Hence, the demoulded samples were stored in the laboratory until mechanical test was performed at 7 and 28 days.

2.3 Characterization of consolidated geopolymers

2.3.1 Setting time. The initial and final setting times of the fresh geopolymer pastes were measured using the Vicat's apparatus. The needle used was 1.00 ± 0.005 mm in diameter. This test was carried out in the laboratory at room temperature (20 ± 3 °C, with a relative humidity of 60%). This test was performed according to the EN196-3 standard.[44] For each formulation three measurements were taken and the average value represents the setting time with standard deviation in bars.

2.3.2 Flowability test. The Flowability test method was conducted using a small cone apparatus, selected from a previous study.[45,46] The small cone has a bottom diameter, top diameter and height of 38 mm, 19 mm and 57 mm, respectively. For each formulation three measurements were taken and the average value represents the flow with standard deviation in bars.

2.3.3 Sorptivity test. The rate of water penetration by capillary suction into the geopolymer binders were measured by sorptivity test in accordance with ASTM C 642.[47] For this test the measurements were taken on cylindrical samples by immersing one side (10 mm) in water at room temperature according to previous study.[48,49] The measurements were performed at 20 ± 3 °C and relative humidity 60%. Three from each formulation were used during the measurements.

2.3.4 Fourier transform infrared spectroscopy (FTIR). To collect information on the structure and composition of the samples, the attenuated total reflectance (ATR)-Fourier-transform infrared spectroscopy (FTIR) technique was used. This was accomplished with a PerkinElmer (UK) Spectrum Two instrument operating in the wavenumber range 400 to 4000 cm^{-1} with a resolution of 4 cm^{-1}.

2.3.5 X-ray diffraction (XRD). The XRD analysis was conducted with a Bruker D8 Advance X-ray diffractometer (Berlin,

Germany) operating with a copper target. During the measurements the working voltage and electric current were 40 kV and 40 mA, respectively. While the step scan was 0.02° with a time counting per step of 0.45 seconds. The 2θ range was 5 to 70°. Before running the analysis, the collected fragments from mechanical test were ground and sieved at 80 μm.

2.3.6 Scanning electron microscopy (SEM). Samples observed using scanning electron microscopy (SEM, Zeiss Ultra Plus device. Oulu, Finland) coupled with EDS are obtained from the debris collected from samples after the mechanical test was carried out. The acceleration voltage used was 40.0 kV. Prior to the SEM examination, the pieces were first mounted in epoxy moulds, then polished and coated with carbon. Analyses were carried out using a backscatter electron detector, a 15 kV acceleration voltage, and a working distance of about 8 mm.

2.3.7 Water absorption, apparent porosity and bulk density. Water absorption, porosity and bulk density of the consolidated binders were determined using ASTM C 642.[50] The conditioning methods outlined in the standard were followed and three samples were prepared and tested. The results presented are the average of the three tested samples.

2.3.8 Mechanical properties. The compressive strength was measured on consolidated samples at 7 and 28 days, using a compressive testing machine (Instron 6959 instrument) with a constant displacement rate of 0.5 mm min^{-1}. The results are the average value of 5 tested samples for each formulation. In eqn (4), the letters F, s, and δ stand for the force in Newtons (N), cross-sectional area (mm^2), and compressive strength (MPa), respectively and error bars denote standard deviation of measurements obtained from five specimens.

$$\delta = F/s \quad (4)$$

2.3.9 Mercury intrusion porosimetry (MIP). Pieces collected from the mechanical test were also assessed using Mercury Intrusion Porosimetry (MIP). The binder pieces were used to prepare specimens of ~1 cm^3 of volume for the MIP test. The equipment has two low-pressure ports and one high-pressure chamber. Mercury intrusion porosimetry (Autopore IV9500, Micromeritics, Norcross, GA 30093, USA) was carried out to measure pore size distributions, total pore volume, total pore surface area, *etc.* The measurements were conducted with the following operative conditions: the equilibrium time (10 s) between pressure limits of 345 kPa and 228 MPa that permits to identify capillary pores between 0.006 and 350 μm.

3. Results and discussion

3.1 Laterite's characterization

Fig. 1 shows the X-ray patterns of raw and calcined laterites. The diffractogram of raw laterite (LAT) shows the reflection peaks of kaolinite minerals with broad bands affected by background noise, reflecting the metastability of this kaolinite and the high potential for iron ion intrusion. It is also observed the less pronounced halo peak centred between 18 and 32° 2θ, representing the amorphous phase contained within the calcined

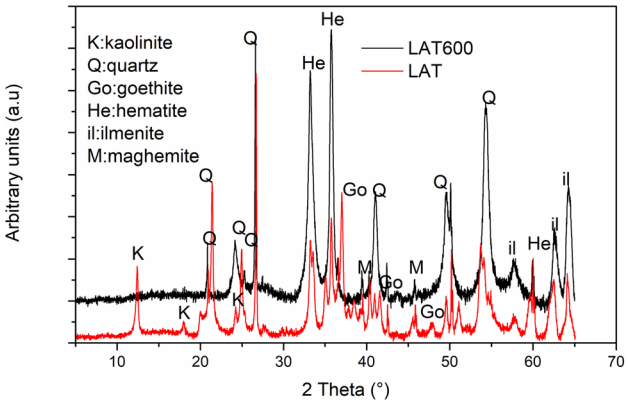

Fig. 1 X-ray patterns of raw laterite (LAT) and calcined laterite at 600 °C (LAT600).

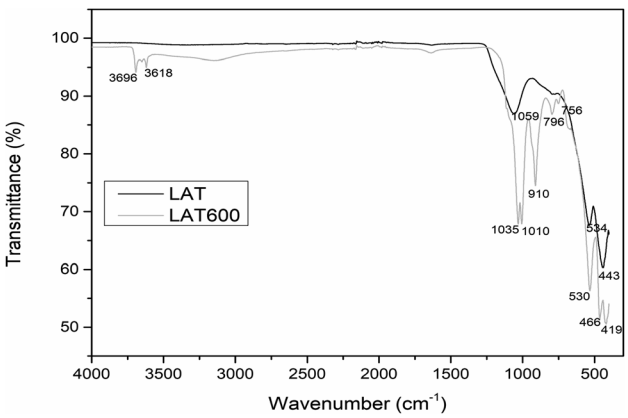

Fig. 2 FTIR spectra of raw laterite (LAT) and calcined laterite at 600 °C (LAT600).

laterite (LAT600). In addition, it was noticed the reflection peaks of the crystalline phases contained in raw and calcined laterite. The main mineral phases using ICDD database, are quartz (SiO_2), hematite (Fe_2O_3), maghemite (γ-Fe_2O_3) and ilmenite ($FeTiO_3$) except kaolinite ($Al_2Si_2O_5(OH)_4$) and goethite (FeOOH) that were only present in raw laterite. During calcination at 600 °C, kaolinite is transformed to metakaolinite which is amorphous in X-ray pattern, while goethite is converted to hematite. The IR spectra of starting and calcined laterite are showed in Fig. 2. The absorption bands located between 3618 and 3696 cm^{-1} are attributed to the vibrational modes of O–H bonds belonging to hydroxylated compounds like goethite and kaolinite contained in raw laterite (LAT).[24,51] These bands disappeared when applied a calcination temperature of 600 °C (LAT600) confirming the total transformation of kaolinite and goethite phases into metakaolinite and hematite respectively.[10,11,15,51]

The absorption peaks at 1035, 1019 and 910 cm^{-1} are assigned to the vibrational modes of Si–O–Si(Al) and Al–OH bonds of kaolinite mineral.[23] Absorption bands located at 1039 cm^{-1} on spectrum of LAT600 is linked to symmetrical stretching of Si–O–Al(Fe) indicating the formation of

amorphous phase requires for the geopolymerization reaction.[52] The absorption bands situated at 796 and 756 cm^{-1} are assigned to Si–O–Si symmetrical stretching as reported by other researchers.[53,54] The last absorption bands appearing at 530, 534, 466, 443 and 419 cm^{-1} are attributed to the vibrational modes of Fe–O, Si–O, Al–O and Fe(Al)–O–Si bonds.[10,34,54–58] These absorption bands confirm the partial replacement in the octahedral site of aluminium cations (Al^{3+}) by iron cations (Fe^{2+} and Fe^{3+}).

3.2 Setting time and flowability

The initial and final setting times recorded on fresh laterite-based geopolymer binders activated with different ratios of alkaline solution to solid precursor content are presented in Table 1, where it can be observed the increase of initial setting time with the increase of alkaline solution to solid precursor ratio. The initial and final setting times are ranged between 96–192 min and 120–220 min, respectively. Both increasing of initial and final setting times with an increase of alkaline solution (AS) to solid precursor (LAT600) ratios from 0.45 to 0.65 is linked to the rise of quantity of alkali activator during the mixing. Hence, the increase of AS/LAT600 mass ratios from 0.45 to 0.65 reduced the viscosity of fresh geopolymer paste that became sticky decreasing the workability followed by the delaying the setting time as seen in Table 1. Similar trend was noticed in previous works where the authors claimed that lower content of alkaline favours the rapid dissolution of solid precursor resulting in shortest setting time whereas high content in alkaline solution delays the setting time.[59] Setting times are highly dependent on the AS/LAT600 mass ratios; increasing the alkali activator content would enrich the entire system with more fluid silica species within the mixes resulting in a longer setting time.[60,61]

Fig. 3 displays the flowability values of different laterite based geopolymer mixes measured from mini-slump cone according to previous studies.[34,35] As seen from Fig. 3, the flow of laterite based geopolymer increased with the increase in AS/LAT600 mass ratios. The values are 80, 95, 125, 155 and 175 mm, respectively, for geopolymer binders when applied a AS/LAT600 mass ratio of 0.45, 0.50, 0.55, 0.60 and 0.65. Thus, increasing the alkaline solution content reduces the solid precursor (LAT600) content in the mixes. However, the high flow recorded in sample made with ratio of 0.65 compared to that of 0.45 is likely linked to the high content of sodium silicate solution as reported in the existing studies.[62] The obtained

Table 1 Initial and final setting times of laterite based geopolymer samples

AS/LAT600 mass ratios	Initial setting time (min)	Final setting time (min)	Final–initial time (min)
0.45	96	120	24
0.50	110	140	30
0.55	135	165	30
0.60	160	193	33
0.65	192	220	28

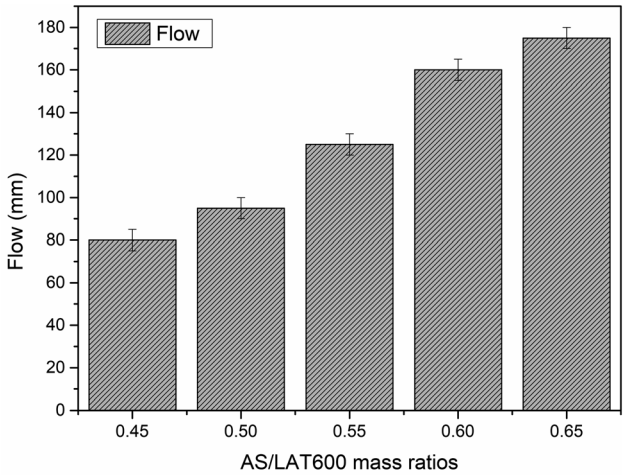

Fig. 3 Flow of fresh laterite based geopolymer pastes for different AS/LAT600 mass ratios.

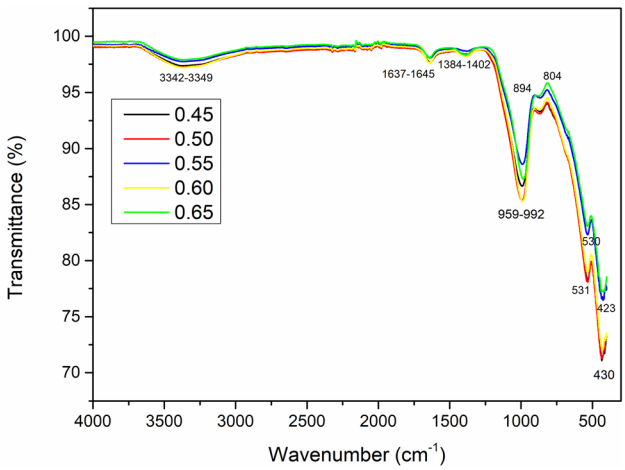

Fig. 4 Infrared spectra of 28 days consolidated laterite based geopolymer with various AS/LAT600 mass ratios.

results are in agreement with the trend of setting times and also quite matches with the observations of other authors using different aluminosilicates (slag, fly ash *etc.*) where they concluded that the ratio of the solid precursor to alkaline activator highly affects the workability, rheology, reactivity and setting time of geopolymer pastes during the synthesis.[23,59,60,62–66]

3.3 Phase's evolution

The infrared spectra of geopolymer binders cured at 28 days consolidated with different AS/LAT600 mass ratios are depicted in Fig. 4. The broad absorption bands appearing in the interval between 3342 and 3349 cm^{-1} are linked to O–H stretching vibrations and the lower bands located between 1637 and 1645 cm^{-1} correspond to bending vibrations of H–O–H belonging to geopolymer structure.[18,67] This implies the absorption of water molecules from the surface of geopolymer network confirming the presence of aluminosilicate hydrate in

geopolymer binder as reported by others author.[18,67] The less pronounced absorption bands in the range of 1384–1402 cm^{-1} are likely due to the stretching vibrations of O–C–O group belonging sodium carbonate, which is formed from reaction of atmospheric CO_2 with unfixed Na^+ ions that migrated out of geopolymer matrix.[34,52,57,58,68] Absorption bands at 959–992 cm^{-1} are attributed to asymmetrical vibrations of Si–O–Al(Fe) bonds. This region in literature suggests the formation of amorphous aluminosilicate binder phase during the geopolymerization reaction.[69–72] The absorption bands appearing at 894 and 804 cm^{-1} are also linked to the stretching of C–O bonds. The last absorption bands located at 530 and 536 cm^{-1} are assigned to vibrational modes of Si–O–Si, Si–O–Al and Fe–O bonds as reported in literature.[10,11,18,24,58]

Fig. 5 exhibits the X-ray patterns of consolidated laterite based geopolymers with various AS/LAT600 mass ratios cured at 28 days. The halo diffused peak appearing in the calcined laterite (LAT600) from 18 to 32° 2θ, shifted to 20 and 40° (2θ) after alkaline activation suggesting the newly formed amorphous phase responsible for the strength development. The reflections attributable to crystalline phases such as: quartz (α-SiO_2), hematite (Fe_2O_3), maghemite (γ-Fe_2O_3), and ilmenite ($FeTiO_3$) in calcined laterite (LAT600) were identified. This suggests that these mineral phases have not totally involved in geopolymerization reaction. However, it is observed the formation of fayalite ($FeSiO_4$) as newly formed phase within the geopolymer samples according to XRD analysis. The presence of fayalite on different diffractograms indicates that some iron mineral compounds would have been altered in alkaline medium during the geopolymerization as reported by existing studies on different aluminosilicate with noticeable amount of iron minerals.[73,74] The presence of the peak attributed to carbonates in FT-IR spectra (Fig. 4) complies with the presence of siderite ($FeCO_3$) at around to 26° in 2θ. This compound can be attributed to the appearance of solid/gas reactivity products combining the freshly produced Fe_2O_3 (during the calcination step at about 360 °C[75]) from goethite (FeOOH), with atmospheric CO_2. We have not noticed any trace of efflorescence at the surface of the final products confirming the formation of this new carbonated phases could occur within the volume of the geopolymer.

The presence of concentrated NaOH solution slightly increase the solubility of hematite according to the reaction of formation of sodium ferrite, $NaFeO_2$:[76]

$$Fe_2O_3(s) + 2NaOH(aq) \leftrightarrow 2FeO_2^- + 2Na^+ + H_2O \quad (5)$$

as indicated by the constant intensity of the hematite peaks (compare LAT600, Fig. 1).

3.4 Mechanical properties

Fig. 6 illustrates the evolution of compressive strength of consolidated laterite based geopolymer binders cured at 28 days as a function of AS/LAT600 mass ratios. The values are 49.6, 50.4, 54.41, 51.20 and 46.40 MPa, respectively for the samples made with AS/LAT600 mass ratios of 0.45, 0.50, 0.55, 0.60 and 0.65. It is noticed that the mechanical performance increases with the liquid to solid ratio till reaching the maximum at 54 MPa at 0.55. Further increasing in AS/LAT600 mass ratio above 0.55 caused a decrease in compressive strength from 54.41 to 46.40 MPa. We are aware that these differences in the mechanical performance of the consolidated materials are not that relevant since values are very close, yet we are confident that a slight increase at about 0.55 value of the ratio is somehow evidenced by our data. Therefore, applying a AS/LAT600 mass ratio of 0.55 should be considered the optimum of alkaline solution content with best workability that ensured best mechanical performance, allowing the high dissolution of calcined laterite resulting in polycondensation during the geopolymerization reaction. Thus, increasing the AS/LAT600 mass ratio above 0.55 may favour high dissolution of reactive phase from solid precursor but this could have delayed the polycondensation rate of dissolved species as the diffusion became difficult as reported by others authors.[13,21] This would allow the formation of a weak structure justifying the slight reduction in

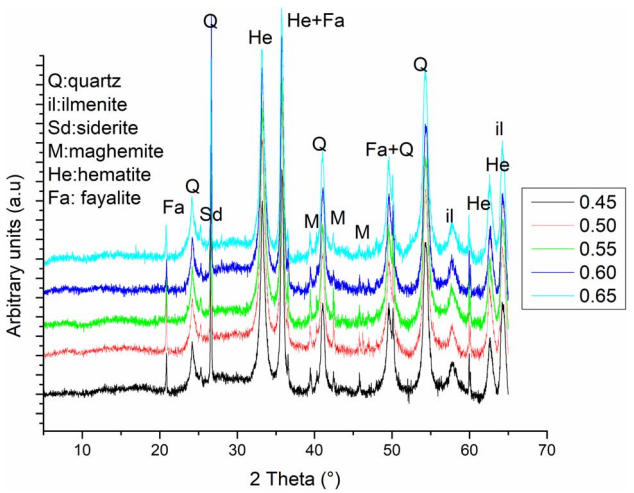

Fig. 5 X-ray patterns of consolidated laterite based geopolymers with various AS/LAT600 mass ratios.

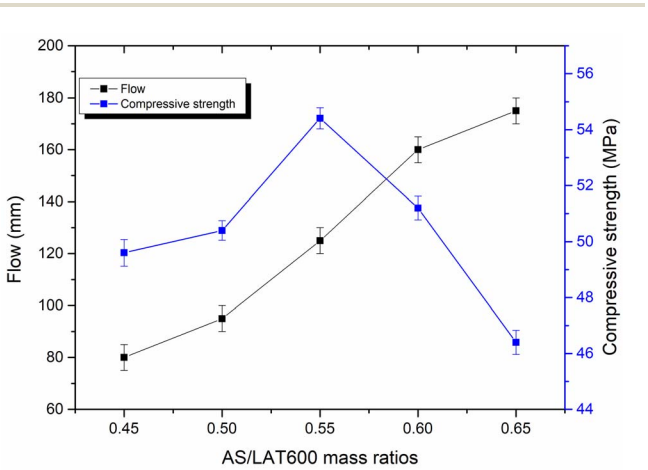

Fig. 6 Compressive strength of geopolymer products cured at 28 days.

strength development. In addition, the high content of alkaline solution used for geopolymer synthesis delaying the polycondensation rate may cause the formation of voids within the microstructure of the hardened geopolymers, affecting the mechanical performance. This quite matches with the findings of Heah *et al.*[23] who stated that using a high amount of alkaline solution medium in the mixture for geopolymer synthesis delays the contact between the activating solution and solid precursor.

3.5 SEM/EDS

Fig. 7 exhibits the SEM images of geopolymer specimens made with AS/LAT600 mass ratios of 0.45, 0.50, 0.55, 0.60 and 0.65, respectively. All the microstructures appear very homogeneous and nearly totally densified. It is noticed the appearance of micro fissures with few accessible voids alongside the micrographs of samples made with AS/LAT600 mass ratios of 0.45, 0.60 and 0.65. The formation of these micro fissures affected the strength development recorded on these samples. The formed binder phase from sample made with 0.45 was not or enough sufficient to allow better cohesion between different particles within the geopolymer matrix compared to specimens made with ratios equal to 0.50 and 0.55. However, using a high AS/LAT600 ratio, above 0.55, the high content of Na^+ within the geopolymer matrix remains unfixed to matrix and it could migrate out and react with CO_2 from atmosphere, justified by the pronounced absorption band close to 1400 cm^{-1} on samples made with 0.60 and 0.65 according to FTIR spectroscopy analysis explained earlier (Fig. 4). This side reactivity of Na^+ ions results in poor and lesser compact structure affecting the mechanical properties.[12,19,20,23] Conversely, using 0.55 of AS/LAT600 mass ratio promoted the high dissolution of solid precursor favouring the important formation of geopolymer binder favourable to the achievement of a strong and densified structure.

Fig. 8–10 highlight the micrographs and elemental map exhibiting the distribution of elements within the matrices of geopolymer samples consolidated with 0.45, 0.55 and 0.65 of

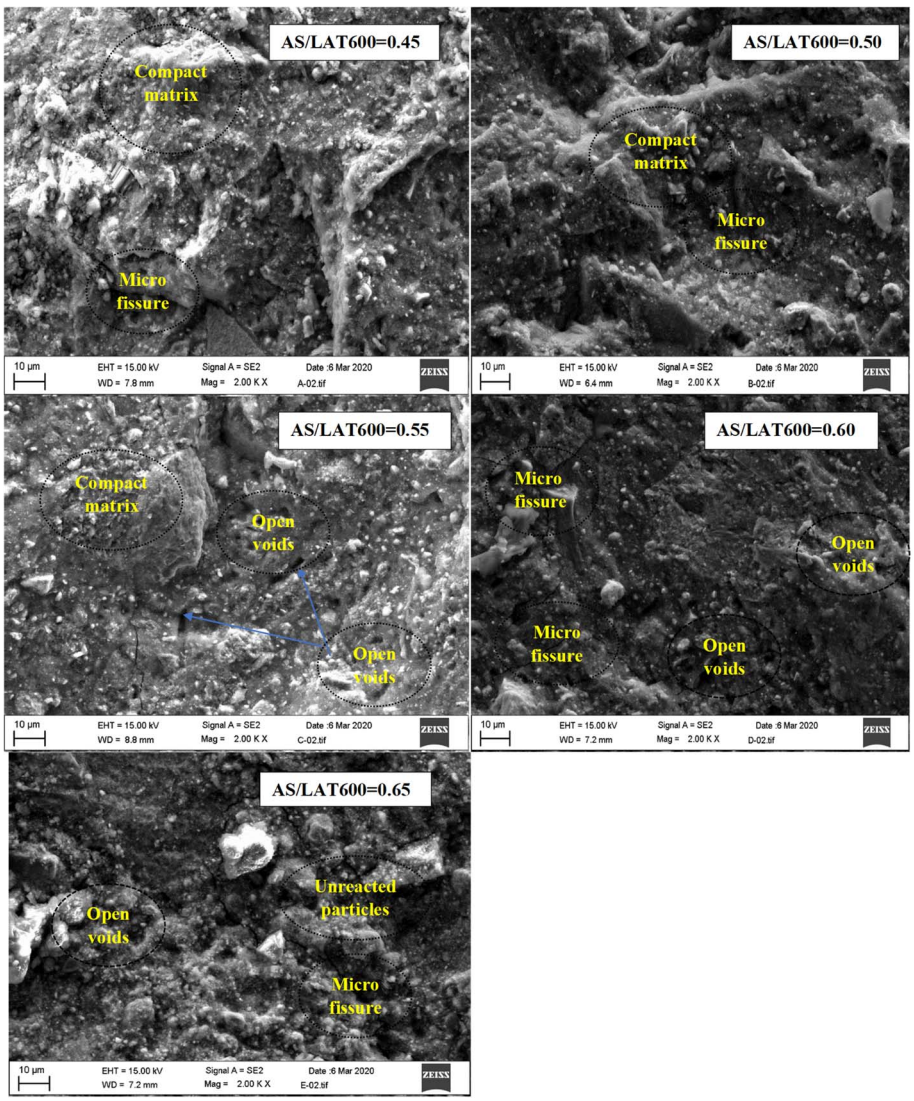

Fig. 7 SEM images of laterite based geopolymer made with different solid/liquid ratios.

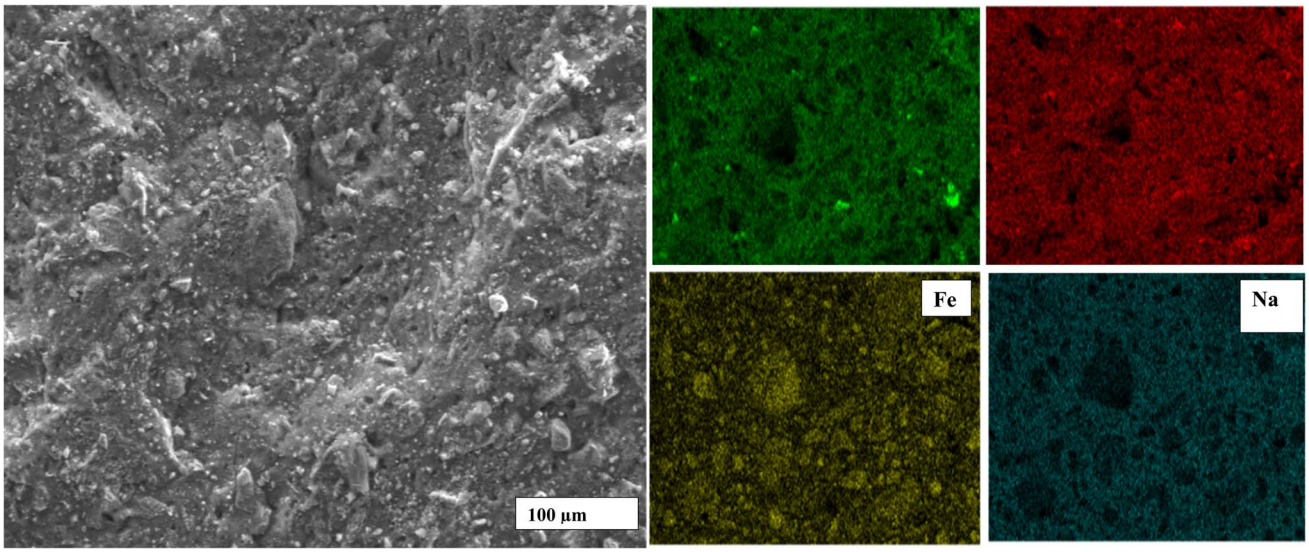

Fig. 8 Micrograph of elemental map of laterite based geopolymer consolidated with 0.45.

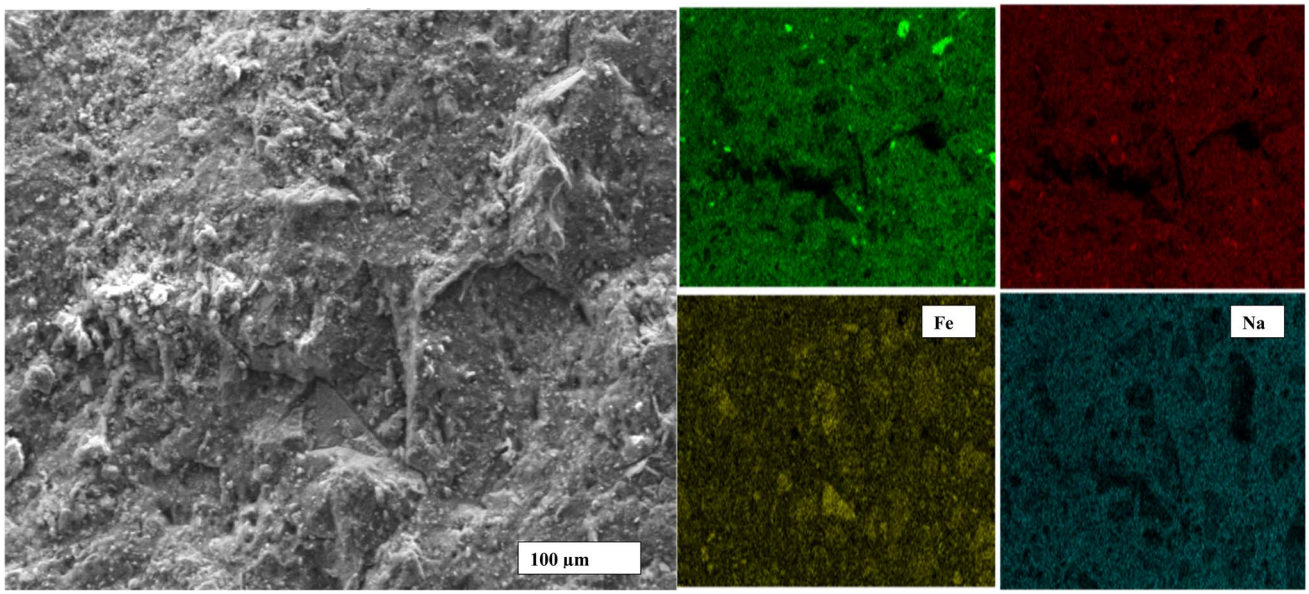

Fig. 9 Micrograph of elemental map of laterite based geopolymer consolidated with 0.55.

alkaline solution to calcined laterite powder mass ratio, respectively. From Fig. 8 and 9, it is observed the homogeneous distribution of the main atoms like Na, Si, Al, Fe alongside the micrographs of samples made with 0.45 and 0.55 compared to that of 0.65 (Fig. 10). This homogeneous distribution is linked to the geopolymer binder which is enough produced in geopolymer sample labelled 0.55 ensuring the high strength achieved. Whereas in geopolymer sample made with alkaline solution to calcined laterite powder ratio of 0.65 the distribution is not similar to that of 0.55, this quite explains the low polycondensation or polymerization between different oligomer species that did not ensure the high production of geopolymer binder require for the strength development. Finally, the observed heterogeneous distribution of Na, Si, Al, Fe atoms in the matrix of sample made with 0.65 (Fig. 10) is due to the low geopolymerization reaction. From this mapping the geopolymer binder is mainly amorphous sodium-polysialiate or polyferrosialate binding phase types.[33,42]

3.6 Sorptivity

The results of sorptivity test applied on calcinated laterite based geopolymer samples made with AS/LAT600 mass ratios of 0.45, 0.50, 0.55, 0.60 and 0.65 are presented in Fig. 11. The sorptivity parameters are reported in Table 2. From Fig. 11, it is observed a rapid increase of water rate penetration at early time up to 50 min in all the laterites based geopolymer series consolidated

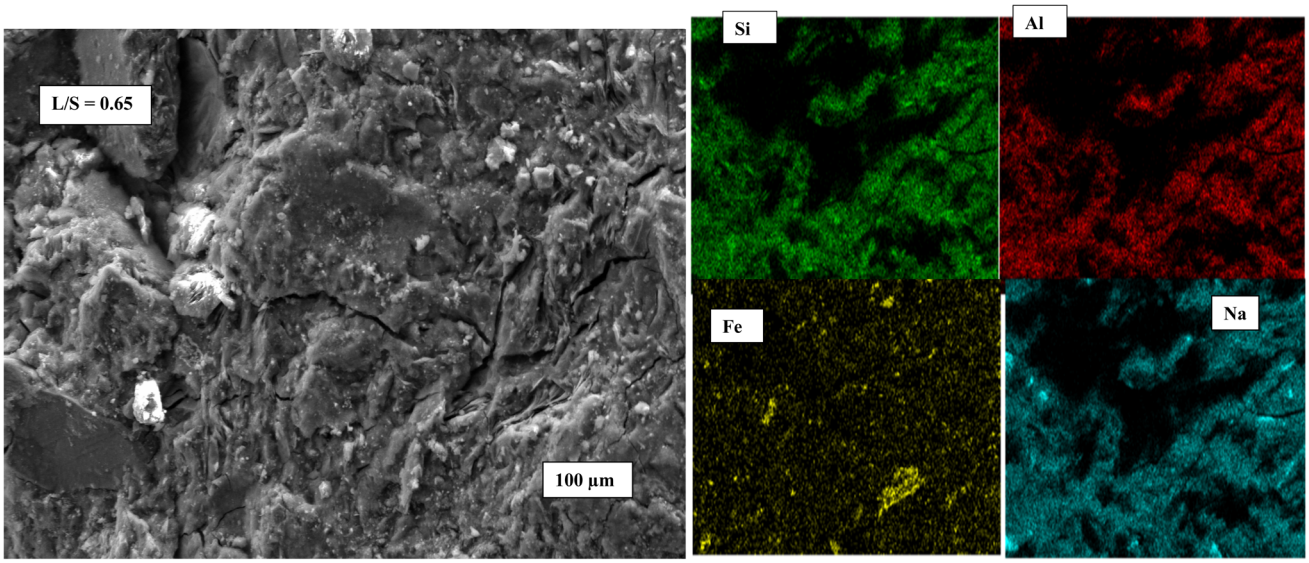

Fig. 10 Micrograph of elemental map of laterite based geopolymer consolidated with 0.65.

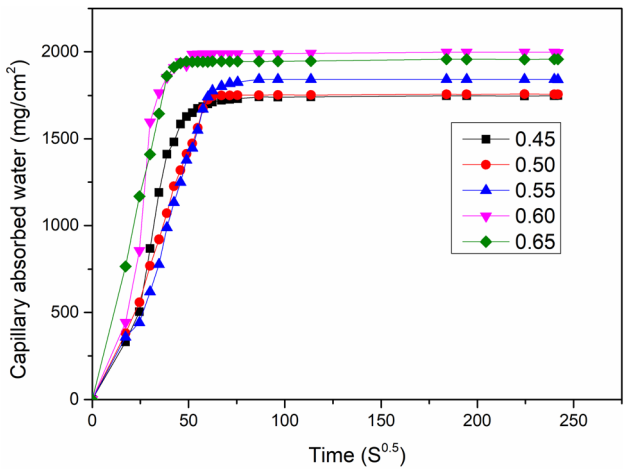

Fig. 11 Capillary water absorption test of laterite based geopolymer binders cured at 28 days.

which became slow and almost constant as evident in the slopes of the lines as shown in Fig. 11. In addition, it is also noticed the increase in capillary absorbed water with the rise of AS/LAT600 mass ratios above 0.55. This is likely to be related to the high content of alkaline that delay the polycondensation rate of dissolved calcined laterite in contact of alkaline solution allowing the formation of poor or less compact structure exhibiting the open voids and micro fissures alongside the matrix favourable for suction of liquid water during the measurements. This is justified by the increase in total water absorption from 19.80 to 24.20% as seen in Table 2. Hence for the samples made with AS/LAT600 mass ratio of 0.45, 0.50 and 0.55, which exhibited low capillary water absorption coefficient and total water absorption compared to those made with 0.60 and 0.65 (Table 2). This result is in agreement with the trend of mechanical strength recorded on geopolymer series.

3.7 Water absorption, apparent porosity and bulk density

Fig. 12 depicts the data of water absorption, porosity and bulk density recorded consolidated geopolymer specimens cured at 28 days. It appears that the water absorption and porosity increase with the rise of AS/LAT600 mass ratios from 20 to 23% and 36 to 46%, respectively. Such increase is explained by the fact that rising the AS/LAT600 mass ratios from 0.45 to 0.65 led appear progressively the formation of voids and pores within the matrix able to retain water when samples are immersed in water for the test. Hence, using a high AS/LAT600 mass ratio displayed the formation of less compact geopolymer matrix with accessible voids that caused the reduction in mechanical performance and justifying the rise of water absorption and porosity. However, the bulk density of synthesized geopolymer remains almost constant close to 2.23 g cm^{-3} on the samples made with 0.45, 0.50, 0.55 and 0.60. While it is noticed a slight

Table 2 Physical parameters from sorptivity test recorded on consolidated geopolymers

Geopolymer samples (mass ratio)	0.45	0.5	0.55	0.60	0.65
Capillary water absorption coefficient, K (mg cm^{-2} $S^{0.5}$)	9.50 ± 0.08	9.55 ± 0.94	9.76 ± 0.35	10.86 ± 0.01	10.64 ± 0.01
Coefficient correlation, r	0.93 ± 0.06	0.92 ± 0.03	0.98 ± 0.03	0.92 ± 0.06	0.93 ± 0.01
Total water absorption (%)	19.80 ± 0.05	20.56 ± 0.01	21.59 ± 0.65	23.92 ± 0.09	24.21 ± 0.05
Bulk density (g cm^{-3})	2.21 ± 0.07	2.22 ± 0.073	2.22 ± 0.07	2.23 ± 0.07	2.14 ± 0.06

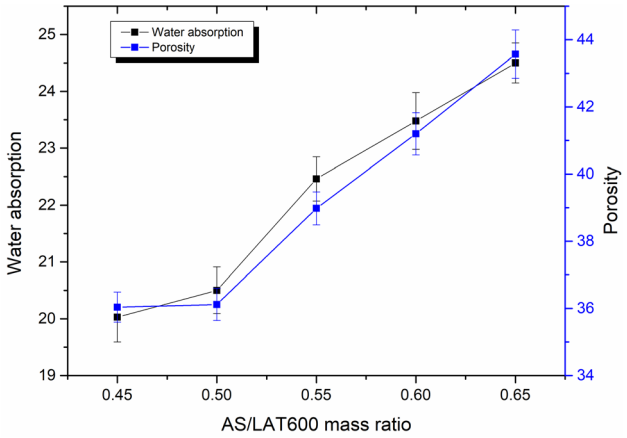

Fig. 12 Water absorption and porosity of laterite based geopolymer binders.

decrease on sample made with 0.65 reaching 2.14 g cm^{-3}. This decrease is probably linked to the open voids that occurred within the matrix rendering this sample a bit lighter compared to others. This trend is in line with the results of water absorption and porosity.

3.8 Mercury intrusion porosimetry

Fig. 13 depicts the results of cumulative intrusion *vs.* log pore diameter (Fig. 13(i)), differential intrusion *vs.* log pore diameter (Fig. 13(ii)) and cumulative pore area *vs.* log pore diameter (Fig. 13(iii)) recorded on selected geopolymer specimens. The cumulative Hg volume intrusion values are 0.11, 0.16, 0.17, 0.20 mL g^{-1}, respectively for geopolymer samples prepared with the AS/LAT600 mass ratio of 0.55, 0.45, 0.50 and 0.60 as shown in Fig. 13(iv). It is observed that the geopolymer sample made with AS/LAT600 mass ratio of 0.55 exhibits lower Hg volume intrusion corresponding to optimum mixture. This agrees with the trend of mechanical strength where the same formulation developed the highest mechanical performance (54.41 MPa). The increase in total volume cumulative intrusion could be linked to the progressive appearance of open voids, micro fissures and pores within the geopolymer matrix affecting the mechanical performance. Hence using lower alkaline solution content limits the propagation of open voids into matrix justifying the formation of dense and compact structure exhibiting high mechanical properties. The lower value of cumulative intrusion recorded (0.11 mL g^{-1}) on geopolymer sample made with 0.55 compared to others is in line with sufficient formed geopolymer binder ensuring better cohesion between different components into the whole system resulting in densified matrix with fewer accessible voids or pores. This is in accordance with high performance achieved.

The pore diameter distribution of geopolymers with the AS/LAT600 mass ratio of 0.55, 0.45, 0.50 and 0.60 is reported in Fig. 13(ii). It ranged between 0.0056–0.0100 μm for samples made with 0.45, 0.50 and 0.55; 0.006–0.17 μm for sample made

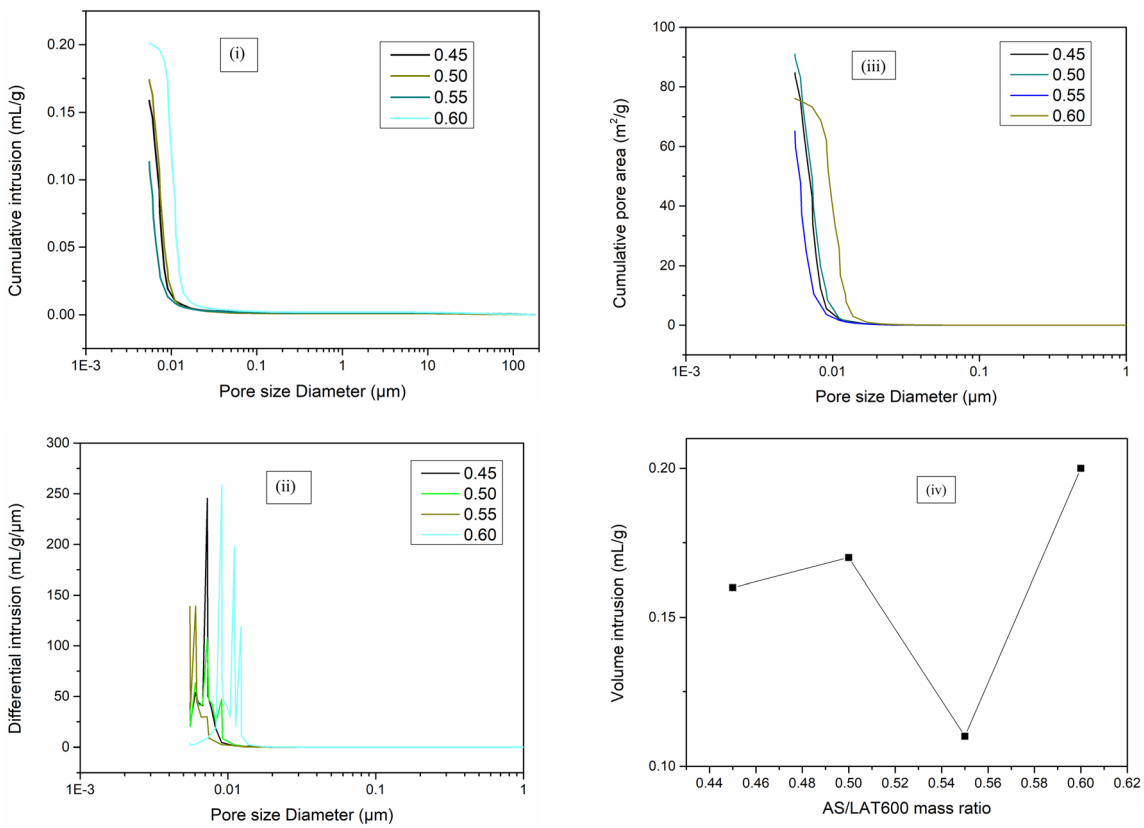

Fig. 13 Cumulative volume intrusion (i), differential intrusion (ii) and cumulative pore area (iii) and (iv) volume intrusion *vs.* AS/LAT600 mass ratio of selected geopolymer specimens.

with 0.60. The threshold pores from 0.006 to 0.017 μm for sample made with 0.60 slightly enlarged compared to others confirms the modifications occurring in the structure when high alkaline solution content is used.

Fig. 13(iii) exhibits the cumulative pore area of selected geopolymers. It is observed that the cumulative pore area increases from 65.20 to 90.93 $m^2 g^{-1}$ with the rise of AS/LAT600 mass ratio from 0.45 to 0.60. Such jump is probably explained the defect such as open voids, micro fissures and pores occurring into geopolymer matrix. It could be concluded that increasing the AS/LAT600 mass ratio during the synthesis seems to affect the pore size evolution, cumulative intrusion cumulative pore area of geopolymer samples. Similar trend was reported by Vogt *et al.*[17]

4. Discussion

The theoretical chemical composition of geopolymer binder made with different ratios is given in Table 3. From Table 3 it has been demonstrated that increasing the alkaline solution content only affected the Na_2O_3/Al_2O_3 and SiO_2/Fe_2O_3 molar ratios which decreases from 2.00 to 1.40 and from 1.58 to 1.28, respectively. Whereas the H_2O/Na_2O and Al_2O_3/Fe_2O_3 remain almost constant and the values are 4.08 and 0.44, respectively when the alkaline solution content increases. Thus, the strength development from geopolymer made with calcined iron-rich laterite activated with varied content of alkaline solution is like linked to Na_2O_3/Al_2O_3 and SiO_2/Fe_2O_3 molar ratios. The highest mechanical strength (54.41 MPa), lower porosity and water absorption is achieved on sample made with 0.55 having composition of $Na_2O_3/Al_2O_3 = 1.64$ and $SiO_2/Fe_2O_3 = 1.41$. This might be attributed due to chemical equilibrium between Na_2O, Fe_2O_3, Al_2O_3 and SiO_2 involved in the geopolymerization reaction ensuring good polycondensation developing a strong and dense matrix with less open voids. Beyond the alkaline solution/calcined iron-rich laterite ratio of 0.55 it is observed a decrease in compressive strength. Such reduction is likely linked to less close relationship between different calcined iron-rich laterite and alkaline solution reactivity. This result demonstrated that calcined iron-rich laterite plays a role in the release of reactive species generating different network formation as well as the chemical composition. It is also worth noting that the novelty of this study stems from the discovery of a correlation between compressive strength, porosity, water absorption, bulk density and starting mixture reactivity. As a result, the positive effects of the activating solution content on the prepared geopolymer properties can be accepted.

Table 3 Chemical composition of consolidated geopolymer calculated on the basis of the different mixes and the oxides content of raw materials

	Alkaline solution/LAT600 ratio				
Oxides (wt%)	0.45	0.50	0.55	0.60	0.65
SiO_2	20.99	21.25	21.50	21.73	21.94
Na_2O	11.65	11.31	10.97	10.66	10.36
H_2O	47.62	46.18	44.83	43.55	42.34
Al_2O_3	5.80	6.30	6.67	7.07	7.45
P_2O_5	0.06	0.06	0.06	0.07	0.07
SO_3	0.02	0.02	0.02	0.02	0.02
K_2O	0.04	0.04	0.04	0.05	0.05
CaO	0.02	0.02	0.02	0.02	0.02
TiO_2	0.39	0.42	0.45	0.50	0.51
V_2O_5	0.03	0.04	0.04	0.04	0.05
Cr_2O_3	0.04	0.04	0.04	0.05	0.05
MnO	0.01	0.01	0.02	0.02	0.02
Fe_2O_3	13.29	14.32	15.30	16.20	17.06
ZrO_2	0.02	0.02	0.02	0.02	0.02
Total	100	100	100	100	100
Al_2O_3/Fe_2O_3	0.44	0.44	0.44	0.44	0.44
Na_2O/Al_2O_3	2.01	1.81	1.64	1.51	1.40
SiO_2/Fe_2O_3	1.60	1.48	1.40	1.34	1.28
H_2O/Na_2O	4.08	4.08	4.08	4.08	4.08

5. Conclusions

Calcined iron-rich laterite (LAT600) mixed with different alkaline solution to solid precursor mass ratio to produce geopolymer binders. Increasing the AS/LAT600 mass ratio up 0.55 yields good workability, low total pore volume (0.11 mL g^{-1}) and the best compressive strength of 54.41 MPa with densified matrix. Whereas further increase beyond 0.55 improved the dissolution but hinder the polycondensation rate of dissolved particles leading to the formation less compact structure justifying the decrease in compressive strength. The capillary pore and cumulative pore area were mainly much influenced by the alkaline solution (AS) content, less by calcined laterite powder (LAT600). Therefore, geopolymer specimens prepared with the optimal AS/LAT600 mass ratio 0.55 produced an important amount of geopolymer binder which promoted the development of the highest mechanical performance with possible application for building construction. However, more detailed research is required to gain a better understanding of the main governing factors influencing the geopolymer mix procedure.

Conflicts of interest

The authors declare that they have no known competing financial interests or personal relationships that could have appeared to influence the work reported in this paper.

Acknowledgements

This project received the contribution of the FLAIR fellowship African Academic of Science and the Royal Society through the funding No FLR/R1/201402 FLR/R1/201402. The authors also are grateful to Ingessil S. r.l., Verona, Italy, for providing sodium silicate solution.

References

1 J. Davidovits, Geopolymers and geopolymeric materials, *J. Therm. Anal.*, 1989, **35**(2), 429–441, DOI: **10.1007/BF01904446**.

2 A. Mellado, C. Catalán, N. Bouzón, M. V. Borrachero and J. M. Monzó, Payá J, Carbon footprint of geopolymeric mortar: Study of the contribution of the alkaline activating solution and assessment of an alternative route, *RSC Adv.*, 2014, **4**, 23846–23852.

3 R. B. E. Boum, C. R. Kaze, J. G. D. Nemaleu, V. B. Djaoyang, N. Y. Rachel, P. L. Ninla, *et al.*, Thermal behaviour of metakaolin–bauxite blends geopolymer: microstructure and mechanical properties, *SN Appl. Sci.*, 2020, **2**(8), 1358.

4 T. W. Cheng and J. P. Chiu, Fire-resistant geopolymer produced by granulated blast furnace slag, *Miner. Eng.*, 2003, **16**(3), 205–210.

5 P. N. Lemougna, A. Adediran, J. Yliniemi, A. Ismailov, E. Levanen, P. Tanskanen, *et al.*, Thermal stability of one-part metakaolin geopolymer composites containing high volume of spodumene tailings and glass wool, *Cem. Concr. Compos.*, 2020, **114**, 103792.

6 M. Ghanbari, A. M. Hadian and A. A. Nourbakhsh, Effect of Processing Parameters on Compressive Strength of Metakaolinite Based Geopolymers: Using DOE Approach, *Procedia Mater. Sci.*, 2015, **11**, 711–716.

7 C. R. Kaze, H. K. Tchakoute, T. T. Mbakop, J. R. Mache, E. Kamseu, U. C. Melo, *et al.*, Synthesis and properties of inorganic polymers (geopolymers) derived from Cameroon-meta-halloysite, *Ceram. Int.*, 2018, **44**(15), 18499–18508.

8 P. Sturm, G. J. G. Gluth, C. Jäger, H. J. H. Brouwers and H. C. Kühne, Sulfuric acid resistance of one-part alkali-activated mortars, *Cem. Concr. Res.*, 2018, **109**, 54–63.

9 W. M. W. Ibrahim, R. Ahmad, B. T. Coman, M. M. A. B. Abdullah, A. Puskas and V. S. Jaganathan, The Effects of Solid to Liquid Ratio on Fly Ash Based Lightweight Geopolymer, *IOP Conf. Ser.: Mater. Sci. Eng.*, 2020, **877**, 012013.

10 C. R. Kaze, G. L. Lecomte-Nana, E. Kamseu, P. S. Camacho, A. S. Yorkshire, J. L. Provis, *et al.*, Mechanical and physical properties of inorganic polymer cement made of iron-rich laterite and lateritic clay: A comparative study, *Cem. Concr. Res.*, 2021, **140**, 106320.

11 A. G. Mimboe, M. T. Abo, J. N. Y. Djobo, S. Tome, R. C. Kaze and J. G. N. Deutou, Lateritic soil based-compressed earth bricks stabilized with phosphate binder, *J. Build. Eng.*, 2020, **31**, 101465.

12 P. Duxson, J. L. Provis, G. C. Lukey, S. W. Mallicoat, W. M. Kriven and J. S. J. Van Deventer, Understanding the relationship between geopolymer composition, microstructure and mechanical properties, *Colloids Surf., A*, 2005, **269**(1–3), 47–58, DOI: **10.1016/j.colsurfa.2005.06.060**.

13 H. Cheng, K.-L. Lin, R. Cui, C.-L. Hwang, T.-W. Cheng and Y.-M. Chang, Effect of solid-to-liquid ratios on the properties of waste catalyst–metakaolin based geopolymers, *Constr. Build. Mater.*, 2015, **88**, 74–83.

14 C. Rodrigue Kaze, P. Ninla Lemougna, T. Alomayri, H. Assaedi, A. Adesina, S. Kumar Das, *et al.*, Characterization and performance evaluation of laterite based geopolymer binder cured at different temperatures, *Constr. Build. Mater.*, 2021, **270**, 121443.

15 C. R. Kaze, S. Tome, G. L. Lecomte-Nana, A. Adesina, H. Essaedi, S. K. Das, *et al.*, Development of alkali-activated composites from calcined iron-rich laterite soil, *Materialia*, 2021, 101032.

16 E. Kamseu, V. Alzari, D. Nuvoli, D. Sanna, I. Lancellotti, A. Mariani, *et al.*, Dependence of the geopolymerization process and end-products to the nature of solid precursors: Challenge of the sustainability, *J. Cleaner Prod.*, 2021, **278**, 123587.

17 O. Vogt, N. Ukrainczyk, C. Ballschmiede and E. Koenders, Reactivity and Microstructure of Metakaolin Based Geopolymers: Effect of Fly Ash and Liquid/Solid Contents, *Materials*, 2019, **12**(21), 3485.

18 S. Yaseri, G. Hajiaghaei, F. Mohammadi, M. Mahdikhani and R. Farokhzad, The role of synthesis parameters on the workability, setting and strength properties of binary binder based geopolymer paste, *Constr. Build. Mater.*, 2017, **157**, 534–545.

19 N. Yong-Sing, L. Yun-Ming, M. M. A. Bakri Abdullah, N. Hui-Teng, K. Hussin, H. C. Yong, *et al.*, Effect of Solid-to-Liquid Ratio on Thin Fly Ash Geopolymer, *IOP Conf. Ser.: Mater. Sci. Eng.*, 2020, **743**, 012006.

20 Y. M. Liew, H. Kamarudin, A. M. M. A. Bakri, M. Binhussain, M. Luqman, I. K. Nizar, *et al.*, Influence of Solids-to-liquid and Activator Ratios on Calcined Kaolin Cement Powder, *Phys. Procedia*, 2011, **22**, 312–317.

21 Y. M. Liew, H. Kamarudin, A. M. Mustafa Al Bakri, M. Bnhussain, M. Luqman, I. Khairul Nizar, C. M. Ruzaidi and C. Y. Heah, Optimization of solids-to-liquid and alkali activator ratios of calcined kaolin geopolymeric powder, *Constr. Build. Mater.*, 2012, **37**, 440–451.

22 K.-W. Lo, K.-L. Lin, T.-W. Cheng, Y.-M. Chang and J.-Y. Lan, Effect of nano-SiO2 on the alkali-activated characteristics of spent catalyst metakaolin-based geopolymers, *Constr. Build. Mater.*, 2017, **143**, 455–463.

23 C. Y. Heah, H. Kamarudin, A. M. Mustafa Al Bakri, M. Bnhussain, M. Luqman, I. Khairul Nizar, *et al.*, Study on solids-to-liquid and alkaline activator ratios on kaolin-based geopolymers, *Constr. Build. Mater.*, 2012, **35**, 912–922.

24 E. Kamseu, C. R. Kaze, J. N. N. Fekoua, U. C. Melo, S. Rossignol and C. Leonelli, Ferrisilicates formation during the geopolymerization of natural Fe-rich aluminosilicate precursors, *Mater. Chem. Phys.*, 2020, **240**, 122062.

25 R. C. Kaze, L. M. Beleuk à Moungam, M. L. Fonkwe Djouka, A. Nana, E. Kamseu, U. F. Chinje Melo, *et al.*, The corrosion of kaolinite by iron minerals and the effects on geopolymerization, *Appl. Clay Sci.*, 2017, **138**, 48–62.

26 R. C. Kaze, L. M. Beleuk à Moungam, M. Cannio, R. Rosa, E. Kamseu, U. C. Melo, *et al.*, Microstructure and engineering properties of Fe_2O_3(FeO)-Al_2O_3-SiO_2 based geopolymer composites, *J. Cleaner Prod.*, 2018, **199**, 849–859.

27 P. O. Awoyera, J. O. Akinmusuru and J. M. Ndambuki, Green concrete production with ceramic wastes and laterite, *Constr. Build. Mater.*, 2016, **117**, 29–36.

28 P. O. Awoyera, A. R. Dawson, N. H. Thom and J. O. Akinmusuru, Suitability of mortars produced using

laterite and ceramic wastes: Mechanical and microscale analysis, *Constr. Build. Mater.*, 2017, **148**, 195–203.

29 A. Jose and A. K. Kasthurba, Laterite soil-cement blocks modified using natural rubber latex: Assessment of its properties and performance, *Constr. Build. Mater.*, 2021, **273**, 121991.

30 S. I. Fundi, J. W. Kaluli and J. Kinuthia, Performance of interlocking laterite soil block walls under static loading, *Constr. Build. Mater.*, 2018, **171**, 75–82.

31 A. K. Kasthurba, M. Santhanam and H. Achyuthan, Investigation of laterite stones for building purpose from Malabar region, Kerala, SW India - Chemical analysis and microstructure studies, *Constr. Build. Mater.*, 2008, **22**(12), 2400–2408.

32 A. K. Kasthurba, M. Santhanam and M. S. Mathews, Investigation of laterite stones for building purpose from Malabar region, Kerala state, SW India – Part 1: Field studies and profile characterisation, *Constr. Build. Mater.*, 2007, **21**(1), 73–82.

33 C. R. Kaze, J. N. Y. Djobo, A. Nana, H. K. Tchakoute, E. Kamseu, U. C. Melo, *et al.*, Effect of silicate modulus on the setting, mechanical strength and microstructure of iron-rich aluminosilicate (laterite) based-geopolymer cured at room temperature, *Ceram. Int.*, 2018, **44**(17), 21442–21450.

34 J. V. Sontia Metekong, C. R. Kaze, J. G. Deutou, P. Venyite, A. Nana, E. Kamseu, *et al.*, Evaluation of performances of volcanic-ash-laterite based blended geopolymer concretes: Mechanical properties and durability, *J. Build. Eng.*, 2021, **34**, 101935.

35 M. Lassinantti Gualtieri, M. Romagnoli, S. Pollastri and A. F. Gualtieri, Inorganic polymers from laterite using activation with phosphoric acid and alkaline sodium silicate solution: Mechanical and microstructural properties, *Cem. Concr. Res.*, 2015, **67**, 259–270.

36 C. N. Bewa, H. K. Tchakouté, C. H. Rüscher, E. Kamseu and C. Leonelli, Influence of the curing temperature on the properties of poly(phospho-ferro-siloxo) networks from laterite, *SN Appl. Sci.*, 2019, **1**(8), 916.

37 P. N. Lemougna, A. B. Madi, E. Kamseu, U. C. Melo, M.-P. Delplancke and H. Rahier, Influence of the processing temperature on the compressive strength of Na activated lateritic soil for building applications, *Constr. Build. Mater.*, 2014, **65**, 60–66.

38 P. N. Lemougna, K.-t. Wang, Q. Tang, E. Kamseu, N. Billong, U. Chinje Melo, *et al.*, Effect of slag and calcium carbonate addition on the development of geopolymer from indurated laterite, *Appl. Clay Sci.*, 2017, **148**, 109–117.

39 K. Komnitsas, G. Bartzas, V. Karmali and E. Petrakis, Factors Affecting Alkali Activation of Laterite Acid Leaching Residues, *Environments*, 2021, **8**(1), 4.

40 K. Komnitsas, E. Petrakis and G. Bartzas, A novel and greener sequential column leaching approach for the treatment of two different Greek laterites, *Sci. Total Environ.*, 2023, **854**, 158748.

41 K. Komnitsas, E. Petrakis, G. Bartzas and V. Karmali, Column leaching of low-grade saprolitic laterites and valorization of leaching residues, *Sci. Total Environ.*, 2019, **665**, 347–357.

42 R. Y. Nkwaju, J. N. Y. Djobo, J. N. F. Nouping, P. W. M. Huisken, J. G. N. Deutou and L. Courard, Iron-rich laterite-bagasse fibers based geopolymer composite: Mechanical, durability and insulating properties, *Appl. Clay Sci.*, 2019, **183**, 105333.

43 C. Nobouassia Bewa, L. Valentini, H. Kouamo Tchakouté, E. Kamseu, J. N. Yankwa Djobo, M. C. Dalconi, *et al.*, Reaction kinetics and microstructural characteristics of iron-rich-laterite-based phosphate binder, *Constr. Build. Mater.*, 2022, **320**, 126302.

44 British Standard EJB, London, *196-3:(2016) Method of testing Cement: Physical Test*, 2016.

45 F. Collins and J. G. Sanjayan, Early Age Strength and Workability of Slag Pastes Activated by NaOH and Na_2CO_3, *Cem. Concr. Res.*, 1998, **28**(5), 655–664.

46 A. M. Rashad, Influence of different additives on the properties of sodium sulfate activated slag, *Constr. Build. Mater.*, 2015, **79**, 379–389.

47 ASTM, C., *Standard test method for slump of hydraulic-cement concrete*, 2012.

48 J. V. S. Metekong, C. R. Kaze, A. Adesina, J. G. D. Nemaleu, J. N. Y. Djobo, P. N. Lemougna, *et al.*, Influence of Thermal Activation and Silica Modulus on the Properties of Clayey-Lateritic Based Geopolymer Binders Cured at Room Temperature, *Silicon*, 2022, **14**, 7399–7416.

49 R. Nkwaju, J. Djobo, J. Nouping, P. Huisken, J. Deutou and L. J. A. C. S. Courard, Iron-rich laterite-bagasse fibers based geopolymer composite: Mechanical, durability and insulating properties, *Appl. Clay Sci.*, 2019, **183**, 105333.

50 ASTM CJC, *Standard test method for density, absorption, and voids in hardened concrete*, 2013.

51 U. Ghani, S. Hussain, A. Noor ul, M. Imtiaz and S. Ali Khan, Laterite clay-based geopolymer as a potential adsorbent for the heavy metals removal from aqueous solutions, *J. Saudi Chem. Soc.*, 2020, **24**(11), 874–884.

52 C. R. Kaze, T. Alomayri, A. Hasan, S. Tome, G. L. Lecomte-Nana, J. G. D. Nemaleu, *et al.*, Reaction kinetics and rheological behaviour of meta-halloysite based geopolymer cured at room temperature: Effect of thermal activation on physicochemical and microstructural properties, *Appl. Clay Sci.*, 2020, **196**, 105773.

53 E. Galan, P. Aparicio, A. Miras, K. Michailidis and A. Tsirambides, Technical properties of compounded kaolin sample from Griva (Macedonia, Greece), *Appl. Clay Sci.*, 1996, **10**(6), 477–490.

54 I. Lecomte, M. Liégeois, A. Rulmont, R. Cloots and F. Maseri, Synthesis and characterization of new inorganic polymeric composites based on kaolin or white clay and on ground-granulated blast furnace slag, *J. Mater. Res.*, 2003, **18**(11), 2571–2579.

55 H. Mohamed, J. G. N. Deutou, C. R. Kaze, L. M. Beleuk à Moungam, E. Kamseu, U. Chinje Melo, *et al.*, Mechanical and microstructural properties of geopolymer mortars from meta-halloysite: effect of titanium dioxide TiO_2 (anatase and rutile) content, *SN Appl. Sci.*, 2020, **2**(9), 1573.

56 J. N. G. Deutou, V. E. L. S. Kamga, R. C. Kaze, E. Kamseu and V. M. Sglavo, Thermal behaviour and phases evolution during the sintering of porous inorganic membranes, *J. Eur. Ceram. Soc.*, 2020, **40**(5), 2151–2162.

57 S. M. Mustakim, S. K. Das, J. Mishra, A. Aftab, T. S. Alomayri, H. S. Assaedi, *et al.*, Improvement in Fresh, Mechanical and Microstructural Properties of Fly Ash- Blast Furnace Slag Based Geopolymer Concrete By Addition of Nano and Micro Silica, *Silicon*, 2021, **13**, 2415–2428.

58 J. G. D. Nemaleu, R. C. Kaze, S. Tome, T. Alomayri, H. Assaedi, E. Kamseu, *et al.*, Powdered banana peel in calcined halloysite replacement on the setting times and engineering properties on the geopolymer binders, *Constr. Build. Mater.*, 2021, **279**, 122480.

59 N. A. Jaya, Y. M. Liew, C. Y. Heah and M. M. A. B. Abdullah, Effect of solid-to-liquid ratios on metakaolin geopolymers, *AIP Conf. Proc.*, 2018, **2045**(1), 020099.

60 Z. Xu, J. Yue, G. Pang, R. Li, P. Zhang and S. Xu, Influence of the Activator Concentration and Solid/Liquid Ratio on the Strength and Shrinkage Characteristics of Alkali-Activated Slag Geopolymer Pastes, *Adv. Civ. Eng.*, 2021, **2021**, 6631316.

61 K. Gao, K.-L. Lin, D. Wang, C.-L. Hwang, H.-S. Shiu, Y.-M. Chang, *et al.*, Effects SiO_2/Na_2O molar ratio on mechanical properties and the microstructure of nano-SiO_2 metakaolin-based geopolymers, *Constr. Build. Mater.*, 2014, **53**, 503–510.

62 P. Nath and P. K. Sarker, Effect of GGBFS on setting, workability and early strength properties of fly ash geopolymer concrete cured in ambient condition, *Constr. Build. Mater.*, 2014, **66**, 163–171.

63 T. Rahmiati, K. A. Azizli, Z. Man, L. Ismail and M. F. Nuruddin, Effect of Solid/Liquid Ratio during Curing Time Fly Ash Based Geopolymer on Mechanical Property, *Mater. Sci. Forum*, 2015, **803**, 120–124.

64 N. Nikoloutsopoulos, A. Sotiropoulou, G. Kakali and S. Tsivilis, The effect of Solid/Liquid ratio on setting time, workability and compressive strength of fly ash based geopolymers, *Mater. Today: Proc.*, 2018, **5**(14), 27441–27445.

65 M. Romagnoli, C. Leonelli, E. Kamse and M. Lassinantti Gualtieri, Rheology of geopolymer by DOE approach, *Constr. Build. Mater.*, 2012, **36**, 251–258.

66 J. N. Y. Djobo, D. Stephan and A. Elimbi, Setting and hardening behavior of volcanic ash phosphate cement, *J. Build. Eng.*, 2020, **31**, 101427.

67 S. Omar Sore, A. Messan, E. Prud'homme, G. Escadeillas and F. Tsobnang, Stabilization of compressed earth blocks (CEBs) by geopolymer binder based on local materials from Burkina Faso, *Constr. Build. Mater.*, 2018, **165**, 333–345.

68 H. Assaedi, T. Alomayri, C. R. Kaze, B. B. Jindal, S. Subaer, F. Shaikh, *et al.*, Characterization and properties of geopolymer nanocomposites with different contents of nano-CaCO3, *Constr. Build. Mater.*, 2020, **252**, 119137.

69 S. Tome, A. Nana, C. R. Kaze, J. N. Y. Djobo, T. Alomayri, E. Kamseu, *et al.*, Resistance of Alkali-Activated Blended Volcanic Ash-MSWI-FA Mortar in Sulphuric Acid and Artificial Seawater, *Silicon*, 2022, **14**, 2687–2694.

70 S. K. Das, J. Mishra, S. M. Mustakim, A. Adesina, C. R. Kaze and D. Das, Sustainable utilization of ultrafine rice husk ash in alkali activated concrete: Characterization and performance evaluation, *J. Sustainable Cem.-Based Mater.*, 2021, 1–19.

71 S. K. Das, S. M. Mustakim, A. Adesina, J. Mishra, T. S. Alomayri, H. S. Assaedi, *et al.*, Fresh, strength and microstructure properties of geopolymer concrete incorporating lime and silica fume as replacement of fly ash, *J. Build. Eng.*, 2020, **32**, 101780.

72 L. M. Beleuk à Moungam, P. N. Lemougna, R. C. Kaze, H. Mohamed, J. G. Deutou Nemaleu, N. Billong, *et al.*, Synthesis of Volcanic Ash-based Porous Inorganic Polymers Using Biomass as Pore Inducing Agent: Phase Evolution and Descriptive Microstructure, *Silicon*, 2022, **14**, 2595–2608.

73 A. Peys, C. E. White, H. Rahier, B. Blanpain and Y. Pontikes, Alkali-activation of CaO-FeO*x*-SiO_2 slag: Formation mechanism from *in situ* X-ray total scattering, *Cem. Concr. Res.*, 2019, **122**, 179–188.

74 S. Onisei, A. P. Douvalis, A. Malfliet, A. Peys and Y. Pontikes, Inorganic polymers made of fayalite slag: On the microstructure and behavior of Fe, *J. Am. Ceram. Soc.*, 2018, **101**(6), 2245–2257.

75 A. C. Kuncser, I. D. Vlaicu, O. D. Pavel, R. Zavoianu, M. Badea, D. Radu, D. C. Culita, A. M. Rostas and R. Rodica Olar, Soft synthesis and characterization of goethite-based nanocomposites as promising cyclooctene oxidation catalysts, *RSC Adv.*, 2021, **11**, 27589–27602, DOI: **10.1039/D1RA04211D**.

76 K. Ishikawa, T. Yoshioka, T. Sato and A. Okuwaki, Solubility of hematite in LiOH, NaOH and KOH solutions, *Hydrometallurgy*, 1997, **45**, 129–135.